International Journal of Heat and Mass Transfer 52 (2009) 1177–1184

Contents lists available at ScienceDirect

International Journal of Heat and Mass Transfer

journal homepage: www.elsevier.com/locate/ijhmt

A comparison of hyperbolic and parabolic models of phase change of a pure metal

Haibo Liu, Markus Bussmann, Javad Mostaghimi *

Department of Mechanical and Industrial Engineering and Centre for Advanced Coating Technologies, University of Toronto, 5 King's College Road, Toronto, Ont., Canada M5S 3G8

ARTICLE INFO

Article history:
Received 20 February 2008
Received in revised form 22 August 2008
Available online 30 October 2008

Keywords:
Rapid solidification
Non-equilibrium
Undercooling
Relaxation time
Interface tracking
Hyperbolic

ABSTRACT

The solidification history of individual thermal spray particles has been the subject of many experimental and theoretical studies. Yet it is customary to assume that solidification occurs at the equilibrium temperature, and that heat propagates according to Fourier's Law. To account for a finite thermal diffusion speed, a hyperbolic heat conduction equation is usually adopted to analyze heat transfer. However, under certain circumstances, this equation can violate the second law of thermodynamics, and so others have modified the original hyperbolic equation via theories of extended irreversible thermodynamics. In this work, we study non-equilibrium effects of rapid solidification of a pure metal particle, and compare the so-called parabolic, hyperbolic and modified hyperbolic equations for heat transfer, to predict the interface undercooling due to thermal effects and velocity as a function of time, for different relaxation times. Results indicate that differences are limited to the early part of the solidification process, when undercooling is most significant, the interface velocity is highest, and non-equilibrium effects are most evident. As solidification progresses, the non-equilibrium effects wane and solidification can then be properly modeled as an equilibrium process.

1. Introduction

Thermal sprayed coatings are built up from an agglomeration of splats formed by the impact, spread, and solidification of individual molten particles. The solidification history of an individual splat at the deposition zone is a process that, to a large extent, determines the final phase structure of a coating. For example, Fig. 1 illustrates Ni splats deposited onto a stainless steel substrate. Note the variation of microstructure across the splat that we are unable to explain, but that we suspect is related to the relative rates of solidification of Ni at the center and periphery of the splat.

It is well understood that rapid solidification affects the formation of the micro and macro characteristics of a splat, including grain size, grain density, and even splat shape [1,2]. Yet phase change models that assume the solidification front is in local thermal equilibrium continue to be applied to the study of splat solidification (e.g., [3]).

To investigate the effect of undercooling and non-equilibrium crystal growth kinetics in rapid solidification, Wang [4] developed a 1D interface tracking model. By assuming that solidification begins when the interface temperature between the splat and substrate reaches the nucleation temperature (below the equilibrium melting temperature), the interface velocity is then linearly related to the local undercooling via a crystal growth kinetics relationship that is an extra constraint on the governing equations.

Yet even Wang's model of rapid solidification is a simplification, in that it assumes an infinite speed of heat conduction, commonly referred to as parabolic heat conduction. The alternative, so-called hyperbolic models, include a relaxation parameter that is related to a finite speed of heat conduction, that presumably leads to further deviations from equilibrium behavior. Mathematically, the hyperbolic models are fundamentally different than the traditional parabolic model; in this paper, we seek to quantify the differences between these models for the case of pure material phase change. The questions we seek to answer include: What factors contribute to non-equilibrium behavior during rapid solidification? What equations reflect such phenomena? Do non-equilibrium behaviors as described by the hyperbolic and parabolic models change the solutions significantly?

It has been noted that non-equilibrium behaviors during rapid solidification are related to many factors, including the intense heat flux as a splat attaches to a substrate, the corresponding large latent heat release, and the most cited factor, the high interface velocity [5]. To answer the second question, it is well known that the conventional parabolic heat conduction equation (PE) assumes an infinite thermal diffusion speed, via Fourier's Law. But when the velocity of the solidification front is comparable to the actual (finite) diffusion speed, such as can occur in rapid solidification, an alternative heat conduction equation ought to be applied. Cattaneo [6] first devised such an equation, to replace Fourier's Law, that in turn yields a so-called conventional hyperbolic heat conduction equation (CHE). But this CHE was later shown (in some extreme circumstances) to yield a negative entropy-production rate per

* Corresponding author. Tel.: +1 416 978 5604; fax: +1 416 978 7753.
E-mail address: mostag@mie.utoronto.ca (J. Mostaghimi).

0017-9310/$ - see front matter © 2008 Elsevier Ltd. All rights reserved.
doi:10.1016/j.ijheatmasstransfer.2008.08.030

Nomenclature

B,E,F,H,S	arrays
b	splat thickness [m]
C	heat wave propagation velocity [m s^{-1}]
c	specific heat capacity [J kg^{-1} K^{-1}]
D	mass diffusivity [m^2 s^{-1}]
D_0	self-diffusivity [m^2 s^{-1}]
e	internal energy [J mol^{-1} K^2]
h	heat transfer coefficient [W m^{-2} K^{-1}]
L	latent heat of solidification [J kg^{-1}]
p	mesh density factor
$\vec{q}$	heat flux [W m^{-2}]
Q	dimensionless heat flux
r	radius [m]
R	gas constant [J mol^{-1} K]
s	entropy [J mol^{-1} K]
T	temperature [K]
T_m	equilibrium melting temperature [K]
T_n	nucleation temperature [K]
u	local energy per unit mass [J mol^{-1} K^2]
u_s	speed of sound in the melt [ms^{-1}]
V_D	mass diffusion velocity [ms^{-1}]
V_i	interface velocity [ms^{-1}]

Greek symbols:

α	thermal diffusivity [m^2 s^{-1}]
β	dimensionless Boltzmann constant
$\Delta\eta$	dimensionless mesh size
ΔG	total Gibbs free energy [J mol^{-1}]
ΔG_{am}	activation energy for molecular migration [J mol^{-1}]
ΔH_M	heat of fusion [J mol^{-1}]
ΔS	entropy of crystallization [J mol^{-1} K]
ΔT_i	interface undercooling [K]
ε	interface location [m]
η	dimensionless coordinate
θ	dimensionless temperature
κ	thermal conductivity [W m^{-1} K^{-1}]
μ_k	linear kinetics coefficient [ms^{-1} K^{-1}]
ρ	density [k g^{-3}]
σ	entropy production rate [J mol^{-1} kg m^{-3}]
τ	relaxation time [s]

Subscripts and Superscripts:

i	interface
j	solid or liquid phase
L	liquid
S	solid
n	time level
*	dimensionless

unit volume [7], by predicting heat conduction from cold to hot, and temperatures below absolute zero. Based on theories of irreversible thermodynamics, modified hyperbolic heat conduction equations (MHE) have been developed to remedy the defects [8].

In the thermal spray process, the solidification front moves rapidly with time, and hence, this is a Stefan problem. A linear relationship between undercooling and interface velocity (often referred to as the dynamic interface condition) is an extra constraint that is often applied [4]. Solutions to the three equations (PE, CHE and MHE) plus the dynamic interface condition, when applied to rapid solidification, have not been compared, nor have solutions been presented that predict interface velocity for hyperbolic models. Analytical solutions are generally unavailable when the interface velocity is linearly related to undercooling, and thus the equations must be solved numerically. Mullis [9] proposed the hyperbolic equivalent of directional solidification to solve the energy equation utilizing a moving coordinate system, but simplified the CHE by assuming a quasi-steady front moving at constant velocity as solidification progressed. Sobolev [10] and Galenko [11] applied the CHE to a concentration field to simulate rapid solidification of a binary alloy using a stable moving coordinate system. Yet in reality, the interface velocity varies dramatically at the onset of rapid solidification, and in this work, we solve for that variation.

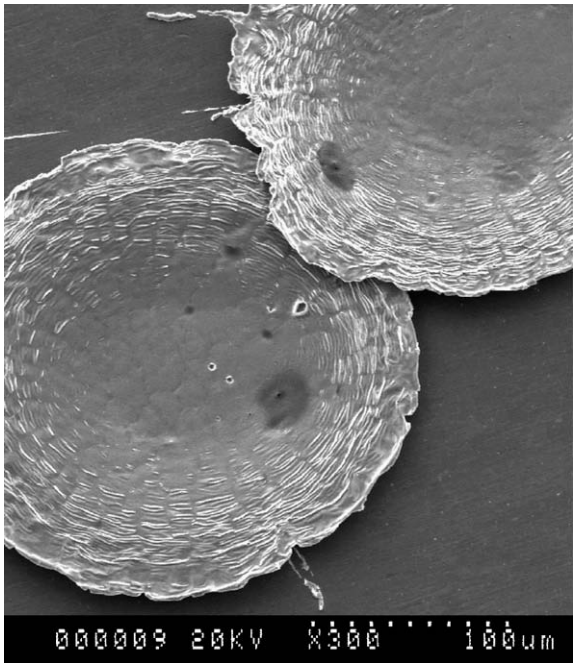

Fig. 1. Micrograph of a Ni splat on stainless steel.

In order to solve these equations numerically, the interface tracking method of Wang [4] that was used to solve the PE [1] has been applied to solve the hyperbolic ones. MacCormack's predictor-corrector method is applied to solve the different equations [5]. At the solidification front, in order to track the interface velocity, the traditional energy balance conditions are incompatible with the hyperbolic equations, and so energy conservation conditions are derived based on the hyperbolic equations, the dynamic interface condition, and a heat flux balance at the interface.

Building on Wang's model [4], we present numerical solutions of the PE, CHE and MHE models applied to the rapid solidification of a pure metal. The effect of varying the relaxation time is investigated, as this is deemed by some (e.g. [Galenko]) to be a critical term especially at the onset of rapid solidification. The results of parabolic and hyperbolic solidification are compared, and serve to clarify whether finite-rate heat conduction effects need to be considered when modeling the rapid solidification of pure metal systems.

The physical description of the problem is as follows: a molten particle impacts a cold substrate, which initiates a strong heat flux at the interface. For a characteristic thermal spray particle of

50 μm diameter impacting at 100 m/s, the fluid spread time (~3 μs) will be at least an order of magnitude less than the characteristic solidification time; hence we neglect convective effects in our solidification model. Solidification begins when crystal nuclei reach a critical size. The directional solidification process is described by the PE, CHE, and MHE governing equations, together with compatible boundary conditions at the solid/liquid interface.

2. Physical model and method formulation

In order to solve for non-equilibrium phase change of a pure metal rapidly solidifying on a substrate, we have developed a 1D model similar to that of Wang [4], based on the following assumptions and idealizations:

1. the droplet forms a thin layer of pure metal, with uniform initial temperature;
2. the droplet and substrate are in perfect contact along a stable planar interface;
3. the interface velocity is linearly related to the undercooling;
4. the heat transfer coefficient at the droplet/substrate interface is assumed to be a constant, inferred from experimental measurements;
5. the heat transfer coefficient at the upper surface of the droplet is much smaller than at the droplet/substrate interface; we assume it to be zero;
6. thermal diffusion coefficients are spatially uniform in the liquid and solid, but not equal.

2.1. Mathematical description

When a molten particle impacts a surface, the interface temperature drops to the melting temperature and heterogeneous nucleation begins. In order to form a crystal nucleus which is stable and will continue to grow, the activation energy must be overcome [12]:

$$\frac{\mathrm{d}(\Delta G)}{\mathrm{d}r} = 0 \tag{1}$$

where ΔG is the free energy barrier at the interface and r is the radius of a spherical crystal. During nucleation, the interface temperature drops until the nucleus reaches a critical size and columnar solidification begins. The temperature at this moment can be regarded as the initial undercooling temperature. Since the substrate material, and surface properties such as substrate cleanliness and smoothness, will affect the critical nucleus size, these interface conditions can be represented by introducing a kinetic coefficient μ_k and an undercooling. Details of this approach will be introduced in the next section.

The basis of hyperbolic models of heat conduction is the so-called generalized Fourier's law

$$\vec{q} + \tau \frac{\partial \vec{q}}{\partial t} = -\kappa_j \nabla T_j \tag{2}$$

where the index $j = L$ or $j = S$ refers to the liquid and solid phases, respectively. Where the usual Fourier's Law implies that a heat flux $\vec{q}$ is proportional to the instantaneous thermal gradient, Eq. (2) implies that the heat flux also depends on the history of the solidification process [13], as it assumes that a heat wave propagates with finite velocity. The relaxation time τ can be thought of as the phase-lag between the temperature gradient and the commencement of heat flow in a medium [14].

When Eq. (2) is introduced into an expression for conservation of energy

$$\rho c_j \frac{\partial T_j}{\partial t} + \nabla \cdot \vec{q} = 0 \tag{3}$$

one obtains the wave-based CHE

$$\frac{\partial T_j}{\partial t} + \tau \frac{\partial^2 T_j}{\partial^2 t} = \alpha_j \nabla^2 T_j \tag{4}$$

which includes an extra term [5] when compared to the classical PE

$$\frac{\partial T_j}{\partial t} = \alpha_j \nabla^2 T_j \tag{5}$$

If $\tau = 0$, Eq. (4) reverts to Eq. (5), and then the heat wave propagates with infinite speed, which implies that the influence of a temperature change on one side of a domain propagates instantaneously to the other side. This is physically unrealistic, although in most cases, the relaxation time is so small that the classical PE suffices.

To assess the thermodynamic validity of different models, Barletta and Zanchini [16] derived the following expression for an entropy production rate

$$\sigma = \nabla \cdot \left(\frac{\vec{q}}{T}\right) + \rho \frac{\partial s}{\partial t} \tag{6}$$

and showed that the CHE is inconsistent with the second law of thermodynamics. Specifically, for constant density ρ, the local energy per unit mass can be expressed as $de = Tds$. Combining Eqs. (3) and (6) leads to the following expression for entropy production rate

$$\sigma = -\frac{1}{T^2} \vec{q} \cdot \nabla T \tag{7}$$

Then combining Eqs. (2) and (7) yields a general form of entropy production that includes the heat flux delay

$$\sigma = \frac{1}{\kappa T^2} \left(\vec{q} \cdot \vec{q} + \tau \vec{q} \cdot \frac{\partial \vec{q}}{\partial t} \right) \tag{8}$$

The first term on the right hand side of Eq. (8) shows that local entropy is related to the heat flux entering a system, which is always positive; the second term, on the other hand, can be negative if there is a steep decrease in heat flux. As a result, the sum of the two terms can yield a negative local entropy production rate, and so violate the second law of thermodynamics. Of course, for $\tau = 0$, the entropy production rate for the PE is always positive.

To remedy this defect, Coleman et al. [17] suggested that internal energy e and entropy must satisfy the following relationships, to keep entropy positive

$$\frac{\partial e}{\partial T} = T \frac{\partial s}{\partial T} \tag{9}$$

$$\frac{\partial e}{\partial q} = T \frac{\partial s}{\partial q} + \frac{\tau q}{\kappa T} \tag{10}$$

Incorporating these equations into Eq. (2) yields a modified first law of thermodynamics [17]

$$\vec{\nabla} \cdot \vec{q} + \left[\rho c + q^2 \frac{\mathrm{d}a}{\mathrm{d}T} \right] \frac{\partial T}{\partial t} + 2aq \frac{\partial q}{\partial t} = 0 \tag{11}$$

with

$$a = -\frac{T^2}{2} \frac{\mathrm{d}}{\mathrm{d}T} \left(\frac{\tau}{\kappa T^2} \right) \tag{12}$$

We refer to the system of equations (2) and (10) as the modified hyperbolic heat conduction equations (MHE). By introducing the following dimensionless quantities

$$Q = \frac{\alpha q}{c \kappa T_0}, \quad \theta = \frac{T}{T_0}, \quad t^* = \frac{c^2 t}{2\alpha}, \quad x^* = \frac{cx}{2\alpha} \tag{13}$$

the MHE become

$$\frac{\partial Q}{\partial t^*}+\frac{\partial \theta}{\partial x^*}=-2Q \tag{14}$$

$$\frac{\partial}{\partial t^*}\left[\theta+\frac{Q^2}{\theta}\right]+\frac{\partial Q}{\partial x^*}=0 \tag{15}$$

Similarly, the nondimensional CHE are

$$\frac{\partial Q}{\partial t^*}+\frac{\partial \theta}{\partial x^*}=-2Q \tag{16}$$

$$\frac{\partial \theta}{\partial t^*}+\frac{\partial Q}{\partial x^*}=0 \tag{17}$$

and the PE are:

$$\frac{\partial \theta}{\partial x^*}=-2Q \tag{18}$$

$$\frac{\partial \theta}{\partial t^*}+\frac{\partial Q}{\partial x^*}=0 \tag{19}$$

Combining Eqs. (18) and (19) yields a nondimensional form of Eq. (4)

$$\frac{\partial^2 \theta}{\partial t^{*2}}+2\frac{\partial \theta}{\partial t^*}=\frac{\partial^2 \theta}{\partial x^{*2}} \tag{20}$$

The relaxation time τ for a metallic system is usually estimated to be on the order of 10^{-10} to 10^{-12} s [13], a value that can been determined in different ways. For example, τ can be defined as $\tau = \alpha C^{-2}$ [9]; as thermal conductivity is related to phonon oscillation, Baumeister and Hamill [15] estimated C to be on the order of 1000 ms^{-1} for metallic systems, and to be related to the velocity of sound in the liquid [9], thus yielding a τ on the order of 10^{-11} or less. On the other hand, even for pure metals, Kurz and Fisher [12] point out that "*the transformation of one phase into another requires rearrangement of atoms, this may involve a relatively short-range (atomic) rearrangement to form a crystal structure.*" This leads us to suggest that τ could also be defined as $\tau = DV_D^{-2}$. From this expression, τ based on mass diffusion would be on the order of 10^{-10} and hence larger than that associated with thermal diffusion. The above estimates of τ, related to either phonon oscillation or atom rearrangement, are what we concern ourselves with. In this paper, we consider this range of relaxation times, in order to assess the extent to which the non-equilibrium term impacts solidification.

In order to solve a Stefan problem, a dynamic interface condition is required, which is usually specified as a linear relationship between undercooling and solidification front velocity [12], derived from theories of crystal growth or collision-limited growth. Considering heterogeneous nucleation without a nucleation barrier, the interface velocity associated with crystal growth can be defined as [18–22]

$$V_i=\beta\frac{D_0}{\delta}e^{\frac{-\Delta G_{am}}{kT_i}}\left[1-e^{-\frac{\Delta H_M \Delta T_i}{kT_i T_m}}\right] \tag{21}$$

where $\beta=\left(\frac{\delta}{\lambda}\right)^2\left(\frac{\nu_i}{\nu_L}\right)$ is a factor introduced by Cahn et al. [18,19]. Collision-limited growth theory yields a different equation for interface velocity [4,24,25]

$$V_i=u_s e^{-\Delta S R^{-1}}\left[1-e^{-\frac{\Delta G}{RT_i}}\right] \tag{22}$$

Note, however, that either of Eqs. (21), (22) can be simplified into a linear kinetic relationship related to undercooling

$$V_i=\mu_k(T_m-T_i)=\mu_k\Delta T_i \tag{23}$$

by assuming that deviations of the interface temperature from the equilibrium melting temperature are small [23]. Thus, for example, the linearized form of Eq. (21) implies that μ_k represents $\beta\left(\frac{D_0}{\delta}\right)\left(\frac{\Delta H_M}{kT_m^2}\right)$ [22]. Eq. (22) reduces to Eq. (23) in a similar way.

The dynamic interface condition (Eq. (23)) at the solid/liquid interface is an extra constraint condition on the PE, CHE and MHE; the energy conservation condition is used to verify the interface velocity and ensures that the interface velocity is applied properly, to maintain the heat flux balance at the interface; this condition leads to [26]

$$\rho_S L\frac{d\varepsilon}{dt}=q^- - q^+ \tag{24}$$

where ε is interface location, and q^- and q^+ represent the heat flux on the liquid and solid sides of the melt front, respectively. Differentiating q^- with respect to time, we obtain

$$\frac{dq^-}{dt}=q_x^-\frac{d\varepsilon}{dt}+q_t^- \tag{25}$$

where the interface velocity is $V_i=-\frac{d\varepsilon}{dt}$. Differentiating Eq. (23) yields

$$T_t^-+\frac{d\varepsilon}{dt}T_x^-=-\frac{1}{\mu_k}\frac{d^2\varepsilon}{dt^2} \tag{26}$$

To obtain a similar interface condition for the CHE, we incorporate Eqs. (25) and (26) into Eqs. (2) and (3), and assuming that the liquid and solid have the same density, obtain the following flux balances for the liquid and solid sides of the interface

$$\frac{1}{\rho_s L}\left[\frac{dq^-}{dt}+\frac{1}{\tau}q^-\right]=\frac{c_L}{L}T_x^-\left[\left(\frac{d\varepsilon}{dt}\right)^2-\frac{\alpha_L}{\tau}\right]+\frac{c_L}{L\mu}\frac{d\varepsilon}{dt}\frac{d^2\varepsilon}{dt^2} \tag{27}$$

$$\frac{1}{\rho_s L}\left[\frac{dq^+}{dt}+\frac{1}{\tau}q^+\right]=\frac{c_s}{L}T_x^+\left[\left(\frac{d\varepsilon}{dt}\right)^2-\frac{\alpha_s}{\tau}\right]+\frac{c_s}{L\mu}\frac{d\varepsilon}{dt}\frac{d^2\varepsilon}{dt^2} \tag{28}$$

Differentiating Eq. (24) with respect to time, and incorporating this into Eqs. (27) and (28) yields

$$\frac{c_s-c_L}{L\mu}\frac{d\varepsilon}{dt}\frac{d^2\varepsilon}{dt^2}+\frac{d^2\varepsilon}{dt^2}+\frac{1}{\tau}\frac{d\varepsilon}{dt}=\frac{c_L}{L}T_x^-\left[\left(\frac{d\varepsilon}{dt}\right)^2-\frac{\alpha_L}{\tau}\right]-\frac{c_s}{L}T_x^+\left[\left(\frac{d\varepsilon}{dt}\right)^2-\frac{\alpha_s}{\tau}\right] \tag{29}$$

This is the interface energy conservation condition for the CHE; if $\tau = 0$, this equation reduces to

$$\frac{d\varepsilon}{dt}=\frac{c_L}{L}T_x^-[\alpha_L]-\frac{c_s}{L}T_x^+[\alpha_s] \tag{30}$$

which is the corresponding equation for the PE.

Similar to how Eq. (29) was derived, the interface energy conservation condition for the MHE is given by

$$\begin{aligned}&\frac{c_s-c_L}{L\mu}\frac{d\varepsilon}{dt}\frac{d^2\varepsilon}{dt^2}+\frac{d^2\varepsilon}{dt^2}+\frac{1}{\tau}\frac{d\varepsilon}{dt}=\frac{c_L}{L}T_x^-\left[\left(\frac{d\varepsilon}{dt}\right)^2-\frac{\alpha_L}{\tau}\right]-\frac{c_s}{L}T_x^+\left[\left(\frac{d\varepsilon}{dt}\right)^2-\frac{\alpha_s}{\tau}\right]\\&+\frac{\tau}{\kappa_s\rho L T_i^2}\frac{d\varepsilon}{dt}\left(q^- -\rho L\frac{d\varepsilon}{dt}\right)^2\left(\frac{d\varepsilon}{dt}T_x^+ +\frac{1}{\mu}\frac{d^2\varepsilon}{dt^2}\right)\\&-\frac{\tau}{\kappa_L\rho L T_i^2}\frac{d\varepsilon}{dt}(q^-)^2\left(\frac{d\varepsilon}{dt}T_x^- +\frac{1}{\mu}\frac{d^2\varepsilon}{dt^2}\right)\\&-\frac{2}{\kappa_s\rho L T_i}\frac{d\varepsilon}{dt}\left(q^- -\rho L\frac{d\varepsilon}{dt}\right)\left(q^- -\rho L\frac{d\varepsilon}{dt}+\kappa_s T_x^+\right)\\&-\frac{2}{\kappa_L\rho L T_i}\frac{d\varepsilon}{dt}(q^-)(q^- +\kappa_L T_x^-)\end{aligned} \tag{31}$$

The above energy conservation conditions, Eqs. (29)–(31), serve as interface conditions when solving the CHE, PE and MHE, respectively.

Finally, we need to specify initial and boundary conditions. The initial conditions are:

$$T(x,0)=T_0,\ q=0 \tag{32}$$

and the boundary condition at the upper surface b of the splat is:

$$\frac{\partial T(b,t)}{\partial x} = 0 \tag{33}$$

The focus of this work is on the very early stage of solidification, when non-equilibrium effects are strongest. As a result, we ignore the heat stored in the solidified material, because the thickness of this region is very small, and so we assume that the solidified region only conducts heat. This allows us to treat the solidified region via a simple boundary condition, that we present in the next section.

2.2. Numerical solution and iteration scheme

A common solution strategy can be applied to the three systems of equations (PE, CHE and MHE), and so in what follows we only present the numerical methodology for the CHE.

Rather than solve Eq. (4) numerically, we solve Eqs. (2) and (3), which are two first-order partial differential equations.

We fix the moving solid/liquid interface by transforming the physical coordinate to a computational one (see Fig. 2)

$$\eta = \left(\frac{x}{\varepsilon}\right)^p \tag{34}$$

p adjusts the mesh density in the liquid region [28]; this non-uniform transformation is necessary to solve the system efficiently. The governing equations in the computational coordinate ($0 \leqslant \eta \leqslant 1$) are then the following

$$\rho c \frac{\partial T}{\partial t} - \rho c p \frac{\mathrm{d}\varepsilon}{\mathrm{d}t}\frac{\partial T}{\partial \eta} + p\eta^{\left(\frac{p-1}{p}\right)}\frac{1}{\varepsilon}\frac{\partial q}{\partial \eta} = 0 \tag{35}$$

$$\tau \frac{\partial q}{\partial t} - \tau p \frac{\eta}{\varepsilon}\frac{\mathrm{d}\varepsilon}{\mathrm{d}t}\frac{\partial q}{\partial \eta} + q + p\eta^{\left(\frac{p-1}{p}\right)}\frac{\kappa}{\varepsilon}\frac{\partial T}{\partial \eta} = 0 \tag{36}$$

MacCormack's predictor–corrector scheme was used to solve this set of equations, which can be written in vector form as [5]:

$$\frac{\partial E}{\partial t} + [B]\frac{\partial F}{\partial \eta} + S = 0 \tag{37}$$

where

$$E = \begin{bmatrix} T \\ q \end{bmatrix}$$

$$F = \begin{bmatrix} q \\ T \end{bmatrix}$$

$$S = \begin{bmatrix} 0 \\ q\tau^{-1} \end{bmatrix}$$

$$B = \begin{bmatrix} \frac{p\eta^{\left[\frac{p-1}{p}\right]}}{\rho c \varepsilon} & -\frac{p}{\varepsilon}\cdot\frac{\mathrm{d}\varepsilon}{\mathrm{d}t} \\ -\frac{p\eta}{\varepsilon}\cdot\frac{\mathrm{d}\varepsilon}{\mathrm{d}t} & \frac{p\kappa\eta^{\left[\frac{p-1}{p}\right]}}{\varepsilon} \end{bmatrix}$$

The resulting finite difference equations for the liquid region are then as follows [5,29]

Step 1:

$$\tilde{E}_i^{n+1} = E_i^n - v[B_i^n][F_{i+1}^n - F_i^n] - \Delta\eta S_i^n \tag{38}$$

Step 2:

$$E_i^{n+1} = \frac{1}{2}\{E_i^n + \tilde{E}_i^{n+1} - v[\tilde{B}_i^{n+1}][\tilde{F}_i^{n+1} - \tilde{F}_{i-1}^{n+1}] - \Delta\eta\tilde{S}_i^{n+1}\} \tag{39}$$

Finally, as discussed earlier, on the solid side of the interface we simplified the interface condition to a boundary condition, by calculating the spatial temperature gradient via a harmonic mean, as suggested by Patankar [27]

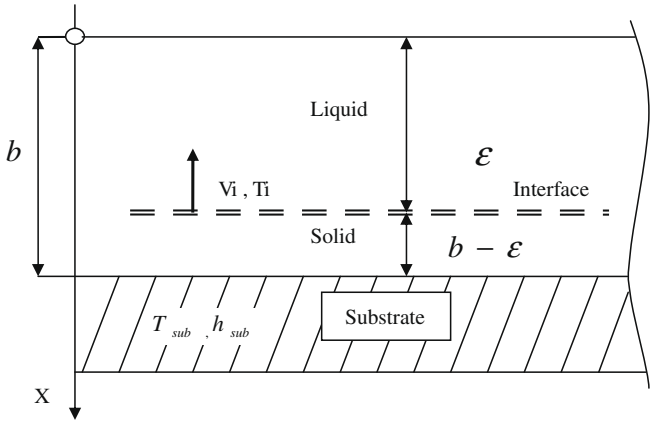

Fig. 2. Schematic of the geometry and coordinate system used in the numerical simulations [14].

$$\frac{\mathrm{d}T}{\mathrm{d}x}\Big|^{+} = \frac{T_i - T_{sub}}{\frac{b-\varepsilon}{\kappa_S} + \frac{1}{h}} \tag{40}$$

T_{sub} is the substrate temperature and κ_S is the thermal conductivity of the solidified material. .

3. Results and discussion

The material properties used in the simulations are given in Table 1. An Al splat of thickness b solidifies on a substrate, as shown in Fig. 2. Wang [30] presented solutions of the PE for this problem; here we present the PE, CHE and MHE, and compare results of the three.

In general, the heat transfer coefficient h in splat cooling ranges from 10^5 to 10^7 W m^{-2} K^{-1} [30]. As we are interested in studying the non-equilibrium effects of rapid solidification, we chose to apply $h = 1.0 \times 10^7$ W m^{-2} K^{-1} in order to increase the interface velocity, which in turn magnifies the effects of non-equilibrium solidification.

To begin, the results of a mesh independence calculation are shown in Fig. 3, for the case of $\tau = 0$ s (parabolic heat conduction), $\Delta T_i = 10$ K, $b = 5.0 \times 10^{-5}$ m, and $\mu_k = 0.05$ m(s K)$^{-1}$ [30]. Note that this splat is much thicker than is usually encountered in a thermal spray coating. To assess mesh independence, we compared three mesh densities: fine ($M = 1000$ nodes, $\Delta = 5.0 \times 10^{-8}$ m), medium ($M = 500$ nodes, $\Delta = 1.0 \times 10^{-7}$ m), and coarse ($M = 250$ nodes, $\Delta = 2.0 \times 10^{-7}$ m). Fig. 3 clearly shows that the three sets of results are nearly identical, as the interface velocity rises from 0.5 ms^{-1} to 2.5 ms^{-1} within 0.11 μs. For the same results, interface temperature versus interface location is illustrated in Fig. 4, which shows that the interface temperature drops from 923 to 885 K within 0.11 μs.

Table 1
Physical properties of Al used in the calculations [30]

Parameter	Units	Value
T_m	K	933.6
D_L	m^2 s^{-1}	5×10^{-9}
κ_L	W m^{-1} K^{-1}	105
κ_S	W m^{-1} K^{-1}	210
c_L	J kg^{-1} K^{-1}	1080
c_S	J kg^{-1} K^{-1}	1180
ρ_L	kg m^{-3}	2390
ρ_S	kg m^{-3}	2550
L	J kg^{-1}	397000

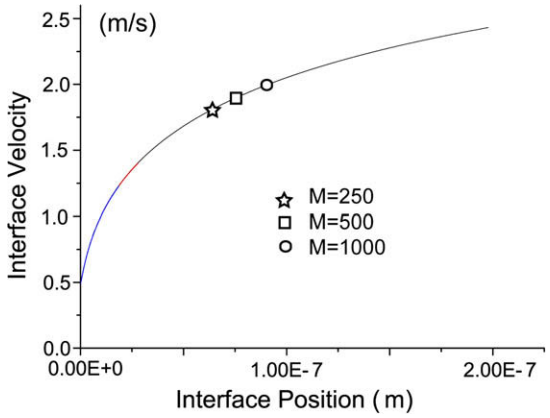

Fig. 3. Interface velocity vs. interface location based on the PE, calculated on various meshes. $T_m = 933$ K, $T_n = 923$ K, $h = 1.0 \times 10^7$ W m^{-2} K^{-1}, $\tau = 0$ s, $\mu_k = 0.05$ m(s K)$^{-1}$.

Mesh independence was then assessed for the PE, CHE and MHE, using the same three meshes; interface velocity versus interface location is presented in Fig. 5 for $\tau = 1.0 \times 10^{-10}$ s. Again, the curves match well, and there is negligible difference between the hyperbolic results and those of the PE solution ($\tau = 0$ s, Fig. 4). From this comparison we can conclude that: (1) the results of the PE, CHE and MHE are mesh independent, and (2) at low interface velocity, with a realistic value of the relaxation time ($\tau = 1.0 \times 10^{-10}$ s), the PE, CHE and MHE yield nearly identical solutions.

We now consider other values of τ; Fig. 6 illustrates results for $\tau = 0$ s, 10^{-8} s, 10^{-7} s and 2×10^{-7} s. Note first that the hyperbolic models predict that the initial velocity decreases as relaxation time increases; for $\tau = 2 \times 10^{-7}$ s, the initial velocity is almost zero. Yet for $\tau = 10^{-8}$ s, the interface velocity profiles differ little from those of the PE. Clearly, when μ_k is small, the initial interface velocity is also small; the results suggest that one can only obtain significant deviations between the hyperbolic and parabolic models with very large values of τ (10^{-7} s). This is an unrealistic relaxation time for a heat conduction problem. Therefore, for realistic relaxation times, (10^{-10}–10^{-12} s), when the interface velocity is very low (0.5 ms^{-1}), the hyperbolic and parabolic models yield the same answers for pure metal solidification. Finally, note that the results of the CHE and MHE are almost identical, even for large values of τ.

Fig. 7 presents PE, CHE, and MHE results of the effect of varying the heat transfer coefficient ($h = 5.0 \times 10^6$ W m^{-2} K^{-1}, 1.0×10^7 W m^{-2} K^{-1} and 5.0×10^7 W m^{-2} K^{-1}), for a large relaxation time

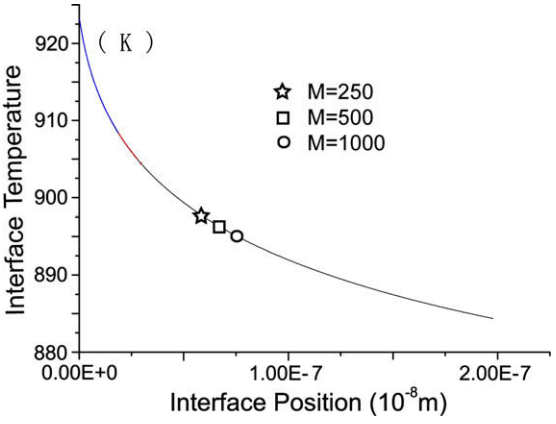

Fig. 4. Interface temperature vs. interface location based on the PE, calculated on various meshes. $T_m = 933$ K, $T_n = 923$ K, $h = 1.0 \times 10^7$ W m^{-2} K^{-1}, $\tau = 0$ s, $\mu_k = 0.05$ m(s K)$^{-1}$.

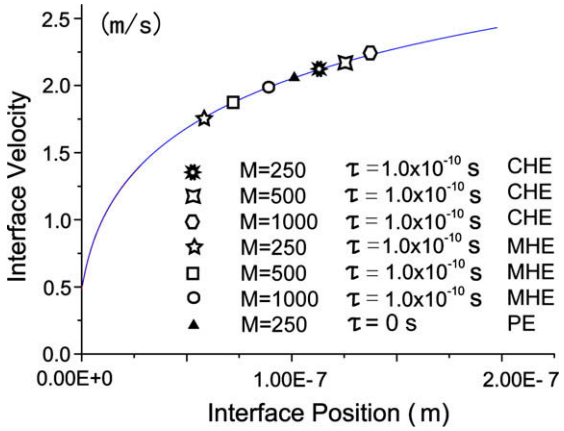

Fig. 5. Interface velocity vs. interface location for the PE, CHE, and MHE equations, calculated on various meshes. $T_m = 933$ K, $T_n = 923$ K, $h = 1.0 \times 10^7$ W m^{-2} K^{-1}, $\mu_k = 0.05$ m(s K)$^{-1}$.

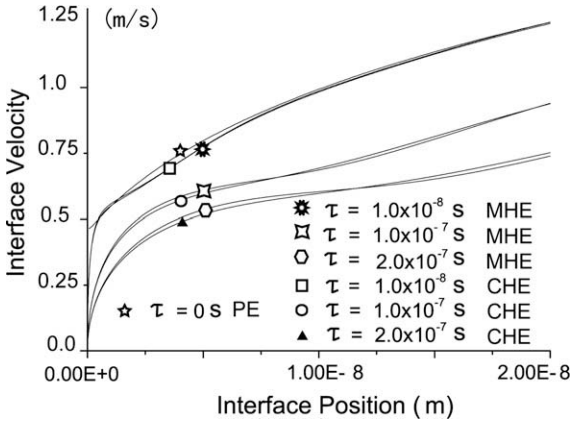

Fig. 6. Interface velocity vs. interface location for various τ. $T_m = 933$ K, $T_n = 923$ K, $h = 1.0 \times 10^7$ W m^{-2} K^{-1}, $\mu_k = 0.05$ m(s K)$^{-1}$.

(10^{-7} s). As can be seen, the minimum deviation between the parabolic and hyperbolic results is for $h = 5.0 \times 10^{-6}$ W m^{-2} K^{-1}. With a larger heat transfer coefficient, the interface velocity increases, which magnifies differences between the hyperbolic and parabolic models, especially at this large value of τ. Note again that the results of the CHE and MHE are nearly identical.

As mentioned previously, τ usually varies between 10^{-10}–10^{-12} s [9] for most heat conduction problems. In such a range, the parabolic and hyperbolic models yield nearly identical results for small V_i. But as interface velocity increases, the deviation increases (Fig. 7), and thus it is worth examining the deviation for relaxation times in the proper range (10^{-10}–10^{-12} s), at high interface velocities.

Recall that Eq. (23) relates V_i to μ_k and the local undercooling ΔT_i. The results of Figs. 3–7 correspond to low values of μ_k and ΔT_i; therefore, the interface velocities are very low (V_i begins at 0.5 ms^{-1}). To more clearly illustrate how higher interface velocities yield non-equilibrium behavior, a larger value of μ_k was used (μ_k can be obtained from either of Eqs. (20) and (21), which yield values of μ_k that can vary by up to two orders of magnitude [28]). Setting $\mu_k = 1.74$ m(s K)$^{-1}$ [28], together with a larger undercooling, Eq. (23) yielded a much higher initial interface velocity for the parabolic model.

Fig. 8 illustrates results for this case. Note first that there are two curves for $\tau = 0$ s (PE model): when $\Delta T = 100$ K and $h = 1.0 \times 10^{-6}$ W m^{-2} K^{-1}, the interface velocity begins at 100 ms^{-1}, but

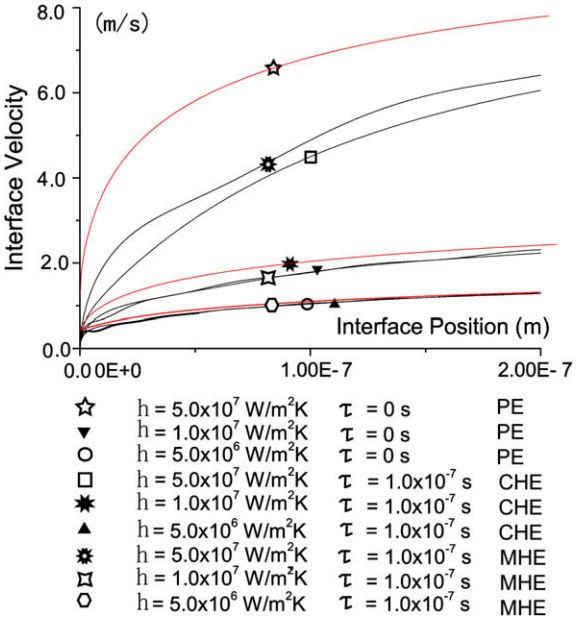

Fig. 7. Interface velocity vs. interface location as a function of the heat transfer coefficient h. $T_m = 933$ K, $T_n = 923$ K, $\mu_k = 0.05$ m(s K)$^{-1}$.

quickly drops to 6 ms^{-1}; when $\Delta T = 0$ K, the interface velocity increases from 0 to 6 ms^{-1}. Clearly, for the parabolic model, the initial interface velocity is determined by ΔT and μ_k; as solidification proceeds, the value of V_i asymptotes to a single value; these results are very similar to those of Wang [30]. The other curves in Fig. 8 show hyperbolic results, which all lie between the two curves of the PE model. The velocities in these cases are initially small, less than that of the parabolic model with same undercooling, then increase dramatically, before approaching the values of the parabolic model. A comparison of these curves also shows that at the beginning of solidification, as τ increases, the velocity decreases, although with time, the curves asymptote to the same value. At the beginning of solidification, when τ decreases, the hyperbolic results are much to the curve of the PE model with the same undercooling. The figure also shows that values of $\tau > 10^{-10}$ s can contribute to non-equilibrium behaviors of solidification, and that these are more obvious at higher interface velocities ($20 \sim 100$ ms^{-1}). Again, the results of the CHE and MHE are nearly identical.

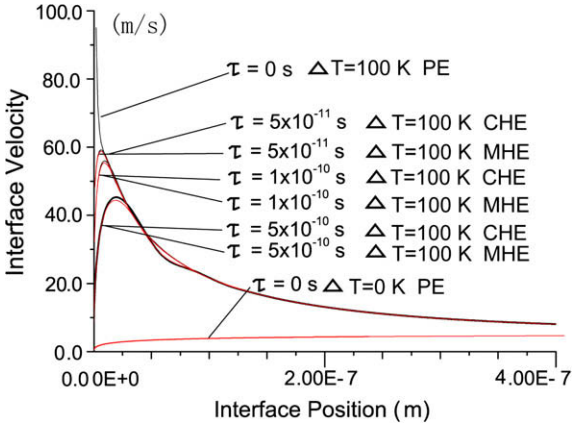

Fig. 8. Interface velocity vs. interface location. $T_m = 933$ K, $T_n = 833$ K or $T_n = 933$ K, $h = 1.0 \times 10^7$ W m^{-2} K^{-1}, $\mu_k = 1.74$ m(s K)$^{-1}$.

Fig. 9 is the same as Fig. 8, but with interface position plotted on a logarithmic rather than a linear scale. Fig. 9 clearly shows the different initial solidification velocities predicted by the hyperbolic and parabolic models. The non-equilibrium phase change of a pure metal is significant only at the very beginning of solidification; as it progresses it converges to the equilibrium result. For most realistic scenarios, since the duration of non-equilibrium effects is very short, such effects can be safely ignored when modeling pure metal solidification. In Fig. 10, the solidification front location is presented versus time, and shows that as τ increases, solidification slows, but again, since the duration is very short ($\sim$0.01 μs), such effects are negligible.

Finally, the results of the CHE model of a thinner splat ($b = 1.0 \times 10^{-5}$ m, $\mu_k = 1.74$ m(s K)$^{-1}$, $\tau = 0$,1.0×10^{-10}, 5.0×10^{-10} s) are shown in Fig. 11. The splat thickness in this case is more representative of that found in a thermal spray coating. The results show that at the initial stage of solidification, the splat thickness does affect the results. Comparing Fig. 8 ($b = 5.0 \times 10^{-5}$ m) and Fig. 10 ($b = 1.0 \times 10^{-5}$ m), one can see that the interface velocity is higher for the thinner splat. For example, when $\tau = 1.0 \times 10^{-10}$, the peak velocity for the thinner splat is around 80 ms^{-1}, while the value for the thinner splat is 70 ms^{-1}. But as V_i approaches the equilibrium velocity, the difference between the two cases diminishes.

4. Conclusions and future work

A 1D interface tracking method has been developed to simulate rapid solidification, based on the PE, CHE and MHE equations. The model takes into account undercooling and non-equilibrium heat flux at the interface. The equations were solved via MacCormack's predictor-corrector method, by transforming the physical coordinate to one that fixes the moving solid/liquid interface.

The numerical results help to understand the non-equilibrium heat wave generated by the hyperbolic equations. The simulations predicted very high interface accelerations at the beginning of solidification. Non-equilibrium effects are related to the relaxation time τ relative to the interface velocity; these effects are negligible for realistic values of τ. We also investigated the role of μ_k; results demonstrated that large values yielded high initial

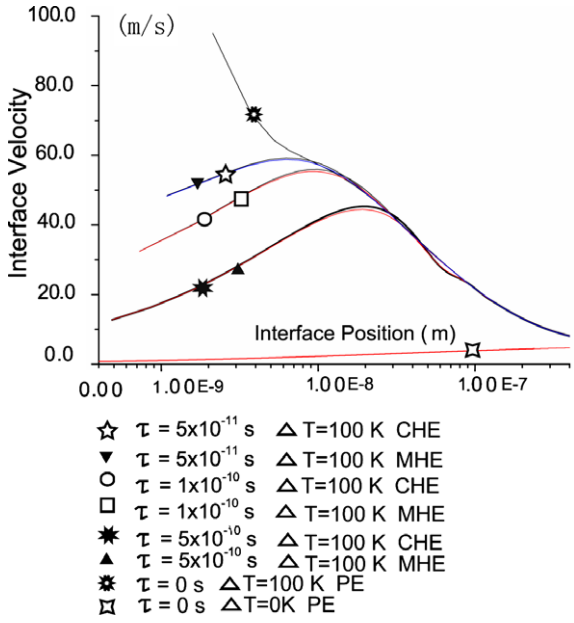

Fig. 9. Same as Fig. 8, but with interface location plotted on a log scale.

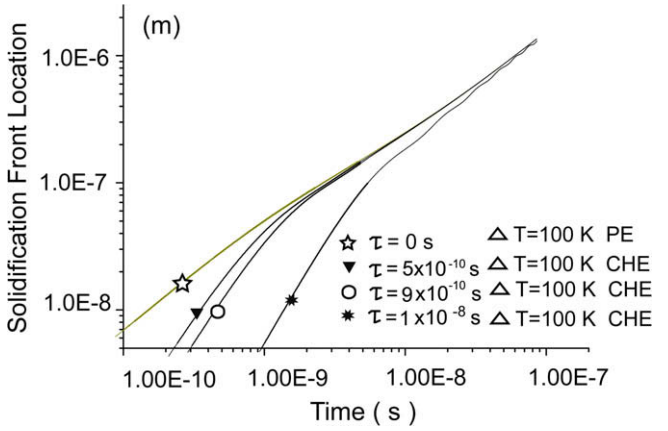

Fig. 10. Solidification front location vs. time, for various τ. $T_m = 933$ K, $T_n = 833$ K, $h = 3.0 \times 10^7$ W m^{-2} K^{-1}, $\mu_k = 1.74$ m(s K)$^{-1}$.

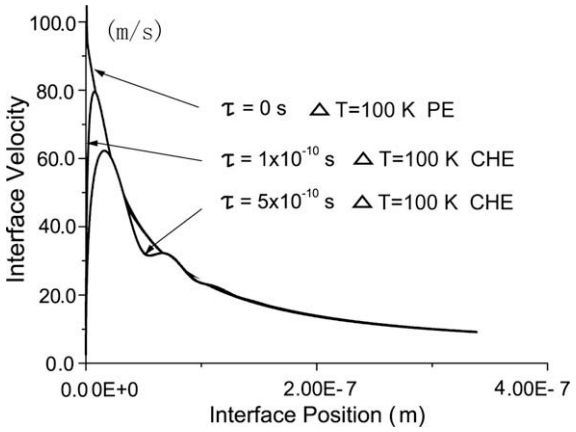

Fig. 11. Interface velocity vs. interface location, varying τ. $T_m = 933$ K, $T_n = 833$ K, $h = 1.0 \times 10^7$ W m^{-2} K^{-1}, $\mu_k = 1.74$ m(s K)$^{-1}$.

interface velocities, which in turn magnify non-equilibrium behavior. Finally, the results show that the CHE and MHE yield nearly identical results.

The work presented here was for rapid solidification of a pure metal. Our future work includes the development of a model for the rapid solidification of an alloy. To compare equilibrium and non-equilibrium binary solidification, a relaxation time term related to the solute diffusion speed will be added to the classical diffusion equations, transforming them from parabolic to hyperbolic. The model will be used to solve the coupled thermal and concentration hyperbolic equations numerically via an iterative interface tracking method built on the one presented here.

References

[1] G.-X. Wang, R. Goswami, S. Sampath, V. Prasad, Understanding the heat transfer and solidification of plasma-sprayed yttria-partially stabilized zirconia coatings, Mater. Manufacturing Process. 19 (2004) 259–272.
[2] Y.K. Chae, J. Mostaghimi, T. Yoshida, Deformation and solidification process of a super-cooled droplet impacting on the substrate under plasma spraying conditions, J. Sci. Technol. Adv. Mater. 1 (2000) 147–156.
[3] M. Pasandideh-Fard, S. Chandra, J. Mostaghimi, A three-dimensional model of droplet impact and solidification, Int. J. Heat Mass Transfer 45 (2002) 2229–2242.
[4] G.-X. Wang, E.F. Matthys, Modeling of nonequilibrium surface melting and resolidification for pure metals and binary alloys, J. Heat Transfer 118 (1996) 944–951.
[5] D.E. Glass, Formulation and solution of hyperbolic Stefan problem, J. Appl. Phys. 70 (1991) 1190–1197.
[6] C. Cattaneo, Sulla conduzione del calore, Atti Sem. Mat. Fis. Univ. Modena 3 (1948) 83–101.
[7] E. Zanchini, Hyperbolic-heat-conduction theories and nondecreasing entropy, Phys. Rev. B 60 (1999) 991–997.
[8] B.D. Coleman, M. Fabrizio, D.R. Owen, On the thermodynamics of second sound in dielectric crystals, Arch. Rational Mech. Anal. 80 (1982) 135–158.
[9] A.M. Mullis, Rapid solidification within the framework of a hyperbolic conduction model, Int. J. Heat Mass Transfer 40 (1997) 4085–4094.
[10] S.L. Sobolev, Rapid solidification under local nonequilibrium conditions, Phys. Rev. 55 (1997) 6845–6854.
[11] P.K. Galenko, D.A. Danilov, Local nonequilibrium effect on rapid dendritic growth in a binary alloy melt, Phys. Lett. A 235 (1997) 271–280.
[12] W. Kurz, D.J. Fisher, Fundamentals of Solidification, third ed., Trans Tech Publications, 1992. pp. 22.
[13] P.K. Galenko, D.A. Danilov, Model for free dendritic alloy growth under interfacial and bulk phase nonequilibrium conditions, J. Cryst. Growth 197 (1999) 992–1002.
[14] J.-R. Ho, C.-P. Kuo, W.-S. Jiaung, Study of heat transfer in multilayered structure within the framework of dual-phase-lag heat conduction model using lattice Boltzmann method, Int. J. Heat Mass Transfer 46 (2003) 55–69.
[15] K.J. Baumeister, T.D. Hamill, Hyperbolic heat conduction equation – a solution for the semi-infinite body problem, J. Heat Transfer 91 (1969) 543–548.
[16] A. Barletta, E. Zanchini, Hyperbolic heat conduction and local equilibrium: a second law analysis, Int. J. Heat Mass Transfer 40 (1997) 1007–1016.
[17] C. Bai, A.S. Lavine, On hyperbolic heat conduction and the second law of thermodynamics, J. Heat Transfer 117 (1995) 256–263.
[18] J.W. Cahn, W.B. Hillig, G.W. Sears, The molecular mechanism of solidification, Acta Metallurgica 12 (1964) 1421–1439.
[19] G.-X. Wang, E.F. Matthys, Mathematical simulation of melt flow, heat transfer and non-equilibrium solidification, Model. Simulation Mater. Sci. Eng. 10 (2002) 35–55.
[20] D. Turnbull, Principles of Solidification, Thermodynamics in Physical Metallurgy, American Society for Metals, 1950. 282–306.
[21] T.W. Clyne, Numerical treatment of rapid solidification, Metall. Mater. Trans. 15B (1984) 369–381.
[22] C.G. Levi, R. Mehrabian, Heat flow during rapid solidification of undercooled metal droplets, Metall. Trans. 13A (1982) 221–234.
[23] J.P. Brazel, E.J. Nolan, Non-Fourier effects in the transmission of heat, in: Proceedings of the Sixth Conference on Thermal Conductivity, Dayton, Ohio, 1967.
[24] R. Ueda, J.B. Mullin, Crystal Growth and Characterization, North-Holland, 1975. 21–32.
[25] J.Y. Tsao, M.J. Aziz, M.O. Thompson, P.S. Peercy, Asymmetric melting and freezing kinetics in silicon, Phys. Rev. Lett. 56 (1986) 2712–2715.
[26] A.D. Solomon, V. Alexiades, D.G. Wilson, J.B. Drake, On the formulation of hyperbolic Stefan problems, Quart. Appl. Math. 43 (1985) 295–304.
[27] S.V. Patankar, Numerical Heat Transfer and Fluid Flow, Hemisphere, 1980. pp. 32–60.
[28] G.-X. Wang, V. Prasad, E.F. Matthys, An interface-tracking numerical method for rapid planar solidification of binary alloys with application to microsegregation, Mater. Sci. Eng. A225 (1997) 47–58.
[29] D.A. Anderson, J.C. Tannehill, R.H. Pletcher, Computational Fluid Mechanics and Heat Transfer, Hemisphere, 1984.
[30] G.-X. Wang, Experimental and numerical study of heat transfer and solidification for molten metal in contact with a cold substrate, PhD thesis, University of California, Santa Barbara, 1995.